Geophysical Research Letters

RESEARCH LETTER
10.1029/2021GL096732

Improving the Vertical Modeling of Tropospheric Delay

Jungang Wang[1,2,3], Kyriakos Balidakis[1], Florian Zus[1], Xiao Chang[1,2], Maorong Ge[1,2], Robert Heinkelmann[1], and Harald Schuh[1,2]

[1]Department of Geodesy, GeoForschungsZentrum (GFZ), Potsdam, Germany, [2]Technische Universität Berlin, Institut für Geodäsie und Geoinformationstechnik, Berlin, Germany, [3]Shanghai Astronomical Observatory, Chinese Academy of Sciences, Shanghai, China

Key Points:

- New method for precise modeling of the zenith hydrostatic and wet delays from the Earth surface up to an altitude of 14 km
- Tropospheric delay vertical modeling precision of better than 3 mm is achieved on a global scale
- The method provides numerical weather model-derived precise tropospheric augmentation correction for real-time space geodetic techniques

Supporting Information:

Supporting Information may be found in the online version of this article.

Correspondence to:

X. Chang,
xiao.chang@gfz-potsdam.de

Citation:

Wang, J., Balidakis, K., Zus, F., Chang, X., Ge, M., Heinkelmann, R., & Schuh, H. (2022). Improving the vertical modeling of tropospheric delay. *Geophysical Research Letters*, *49*, e2021GL096732. https://doi.org/10.1029/2021GL096732

Received 30 OCT 2021
Accepted 28 FEB 2022

Abstract Accurate tropospheric delays from Numerical Weather Models (NWM) are an important input to space geodetic techniques, especially for precise real-time Global Navigation Satellite Systems, which are indispensable to earthquake and tsunami early warning systems as well as weather forecasting. The NWM-based tropospheric delays are currently provided either site-specific with a limited spatial coverage, or on two-dimensional grids close to the Earth surface, which cannot be used for high altitudes. We introduce a new method of representing NWM-derived tropospheric zenith hydrostatic and wet delays. A large volume of NWM-derived data is parameterized with surface values and additional two or three coefficients for their vertical scaling to heights up to 14 km. A precision of 1–2 mm is achieved for reconstructing delays to the NWM-determined delays at any altitudes. The method can efficiently deliver NWM-derived tropospheric delays to a broader community of space geodetic techniques.

Plain Language Summary Precise positioning with microwave-based space geodetic techniques, such as Global Navigation Satellite Systems (GNSS), requires accurate modeling of the atmospheric refraction. Numerical Weather Models (NWM) can provide tropospheric delays with an accuracy of 1–2 cm in zenith direction and are therefore useful for improving the data analysis. However, due to the large data volume to handle, NWM-based products are typically provided only for selected sites, or on a global grid referring to a specific height. We provide an efficient method to represent the vertical profile of tropospheric delay from the Earth surface up to 14 km altitude with a precision of 1–2 mm. The method is used to preserve the precision of NWM-derived tropospheric delays at the altitudes using three to four coefficients per geographic location (longitude, latitude) at the ground. This paves the way of applying the NWM-based accurate tropospheric delays in space geodetic data analysis, especially for global augmentations of real-time GNSS, which play a critical role in the rapid characterization and early warning of geohazards such as earthquake and tsunami, as well as kinematic platforms of high altitudes.

1. Introduction

For the microwave-based space geodetic techniques, the signals propagating through the troposphere are delayed and bent due to the nonvacuum conditions (Böhm & Schuh, 2013). The tropospheric delay is modeled as the sum of the zenith hydrostatic delay (ZHD) and the zenith wet delay (ZWD) mapped to the slant direction. It can be corrected using external products, for instance, in satellite altimetry (Fernandes et al., 2015) and Interferometric Synthetic Aperture Radar (InSAR) (J. Foster et al., 2006), or estimated by setting up unknown parameters, for instance, in Global Navigation Satellite Systems (GNSS) (Emardson & Jarlemark, 1999; Wang et al., 2019) and Very Long Baseline Interferometry (VLBI) (Heinkelmann et al., 2011; Soja et al., 2015). In the latter case, precise external tropospheric delays also contribute to providing a priori values with proper uncertainties and thus help to decorrelate it with other parameters such as station coordinates and receiver clocks. Therefore, they are commonly used to achieve better precision and reliability (Nilsson et al., 2017; Takeichi et al., 2009; Wang & Liu, 2019; Ware et al., 1986), in particular for the regional and global tropospheric augmentation for real-time GNSS (de Oliveira et al., 2016; Hadas et al., 2013; Zheng et al., 2017), which has a broad geophysical applications in enhancing the early warning systems of geohazards such as the earthquake (Grapenthin et al., 2014; Ruhl et al., 2017), the tsunami (Sobolev et al., 2006; Tsushima et al., 2014), and the volcano eruption (Hreinsdóttir et al., 2014; Lee et al., 2015).

Numerical Weather Models (NWM) are important data sources in providing the tropospheric delays for space geodetic techniques. A state-of-the-art NWM provides hourly tropospheric delays with 10-km spatial resolution at

an accuracy of 1–2 cm (Hobiger et al., 2008; Zhou et al., 2020). NWM-derived tropospheric delays are commonly used in Earth observing techniques, including precise GNSS positioning (Lu et al., 2017; Wilgan et al., 2017), VLBI analysis (Eriksson et al., 2014; Hofmeister & Böhm, 2017; Landskron & Böhm, 2019), satellite altimetry (Fernandes et al., 2021; Legeais et al., 2014), and InSAR (Wilgan & Geiger, 2018; Yu et al., 2018). Commonly used NWM-derived tropospheric delay product includes the VMF (Böhm et al., 2006), UNB (Urquhart et al., 2013), and PMF (Balidakis et al., 2018; Zus et al., 2014). As the tropospheric delay is altitude-dependent, it is usually provided either site-specific or as two-dimensional global grids close to the Earth surface. A site-specific product can cover selected geodetic stations only, whereas a huge amount of GNSS stations (e.g., around 17,000 publicly available through Blewitt et al. (2018)) cannot be covered in this way. It is also difficult to provide the epoch-wise tropospheric delay product for kinematic GNSS receivers, especially for those on seaborne and airborne platforms and moving vehicles. Nevertheless, precise tropospheric delays are more important for kinematic GNSS solution especially on moving platforms, which is challenging due to the weak observation geometry and complex environmental errors (J. H. Foster et al., 2009; Penna et al., 2018; Rocken et al., 2005; Vaclavovic et al., 2017; Webb et al., 2016), where the external precise tropospheric information can significantly help enhancing the solution. In contrast, a global grid of two-dimensional tropospheric delays provides a good spatial coverage, but accuracy losses in correcting the delay from the altitude of the grid point to that of the receiver are inevitable.

In this contribution, we aim at efficiently providing precise NWM-based tropospheric delays with a global coverage while minimizing the accuracy loss due to the necessary altitude correction. We present a new algorithm to model the vertical variations of ZHD and ZWD. When adopting the new method based on just a few coefficients, precise tropospheric delays from the surface to an altitude where ZWD vanishes (up to 14 km) are available for users and thus, can be widely used in the space geodetic technique data analysis. We recommend to replace the current ways of providing NWM-based tropospheric delays, which are limited to specific stations or an altitude near the Earth surface, by this new method. We present the derivation of the method in Section 2 and evaluate the modeling performance in Section 3. Thereafter, in Section 4, we summarize and present our conclusions and perspectives.

2. Vertical Modeling of Tropospheric Zenith Delays

The tropospheric delay mainly depends on the atmospheric pressure, temperature, and water vapor content. We first present the vertical modeling of the atmospheric pressure, which subsequently leads to the modeling of zenith hydrostatic and wet delays.

2.1. The Barometric Formula

The barometric formula describes the dependence of atmospheric pressure on altitude and can be written as (Berberan-Santos et al., 1997; Lente & Ősz, 2020):

$$P_h = P_0 \cdot e^{-\frac{Mgh}{RT}} = P_0 \cdot e^{-\frac{h}{H}}; H = \frac{RT}{Mg} \tag{1}$$

where P_h and P_0 denote the atmospheric pressure at the altitude of h and that at sea level, respectively, M is the average molecular mass, g is the gravitational acceleration, R is the general gas constant, and T is the constant temperature. At each geographical location the vertical pressure profile can be described by two coefficients defined on the surface: P_0 and T. Note that for this equation a constant vertical temperature is assumed. The barometric formula considering the standard temperature lapse rate α is (Lente & Ősz, 2020):

$$P_h = P_0\left(1 - \frac{\alpha}{T_0}h\right)^{\frac{Mg}{\alpha R}}; \alpha = -\frac{dT}{dh} \tag{2}$$

where T_0 is the surface temperature. Accordingly, the pressure vertical profile can be described by three coefficients: P_0, T_0, and α. We rearrange Equation 2 as:

$$P_h = P_0 e^{\ln\left(1-\frac{\alpha}{T_0}h\right)^{\frac{Mg}{\alpha R}}} = P_0 e^{\frac{Mg}{\alpha R}\ln\left(1-\frac{\alpha}{T_0}h\right)} \tag{3}$$

which can be approximated with the truncated Taylor series:

$$P_h = P_0 e^{-\frac{Mg}{\alpha R}\sum_{i=1}^{n}\frac{\left(\frac{\alpha}{T_0}h\right)^i}{i}} \tag{4}$$

Note that when truncated at $n = 1$, this equation is the same as Equation 1, that is, assuming a constant vertical temperature. We further restate the series as:

$$P_h = P_0 e^{\sum_{i=1}^{n}\frac{ab^{i-1}h^i}{i}}, a = -\frac{Mg}{\alpha R}\cdot\frac{\alpha}{T_0}; b = \frac{\alpha}{T_0} \tag{5}$$

where the composite parameters a and b are used for simplicity. The reason to rearrange Equation 2 as Equation 5 is that the latter is easier to be linearized and better for fitting the vertical profiles, whereas in Equation 2 both parameters, the base (α and T_0) and the exponent (α), have to be fitted, which could cause numerical issues.

2.2. Modeling the Tropospheric Delay Vertical Profile

Given the atmospheric pressure P_h at the altitude h (in km), the ZHD_h (in m) at latitude φ can be derived as (Davis et al., 1985; Saastamoinen, 1972):

$$ZHD_h = \frac{0.0022768\cdot P_h}{1 - 0.00266\ \cos(2\varphi) - 0.28\times 10^{-6}\cdot h} \tag{6}$$

Inserting Equation 5 into Equation 6, the ZHD at altitude h can be computed knowing the one at reference altitude ZHD_0 (referring to altitude above sea level):

$$ZHD_h = ZHD_0 \cdot e^{\sum_{i=1}^{n}\frac{ab^{i-1}h^i}{i}} \tag{7}$$

where the variation of term $-0.28\times 10^{-6}\cdot h$ (denominator in Equation 6) due to the height difference can be ignored for the majority of space geodetic applications, as the largest value at 14 km is still less than 4×10^{-6}.

The dependence of ZWD_h on the atmospheric pressure can be approximated as (Dousa & Elias, 2014):

$$\frac{ZWD_h}{ZWD_0} = \left(\frac{P_h}{P_0}\right)^{\gamma+1} \tag{8}$$

where γ denotes the exponential decay of the wet delay. Similarly, by inserting Equation 5 into Equation 8, the dependence of ZWD on altitude can be written as:

$$ZWD_h = ZWD_0 \cdot e^{(\gamma+1)\sum_{i=1}^{n}\frac{ab^{i-1}h^i}{i}} \tag{9}$$

Therefore, the coefficients of Equation 7 and Equation 9, respectively, can be fitted to vertical hydrostatic and wet delay profiles from NWM. Note that the above equations are approximations of the vertical profiles, and the tropospheric delays do not always rigorously follow them, especially the wet delay, which can show more fluctuations due to a water vapor vertical variability.

To investigate the impact of the different truncation terms, we fit the ZHD and ZWD separately, both using the form of Equation 7 (ZWD can be formed similar to Equation 7). Numerical tests of 1-year results show that for truncation cases $n = 2$ and $n = 3$, the differences of the root mean square (RMS) of residuals are usually less than 1 mm for both, ZHD and ZWD. Moreover, only ZHD shows an average reduction of 0.4 mm when truncated at $n = 3$ (see Figure S1 in supporting information).

Equation 7 truncated at $n = 3$ can be written as:

$$ZHD_h = ZHD_0 \cdot e^{b_1 h + b_2 h^2 + b_3 h^3} \tag{10}$$

which is rigorously equivalent to Equation 7 if it satisfies:

$$3\cdot b_1 \cdot b_3 = 4\cdot {b_2}^2 \tag{11}$$

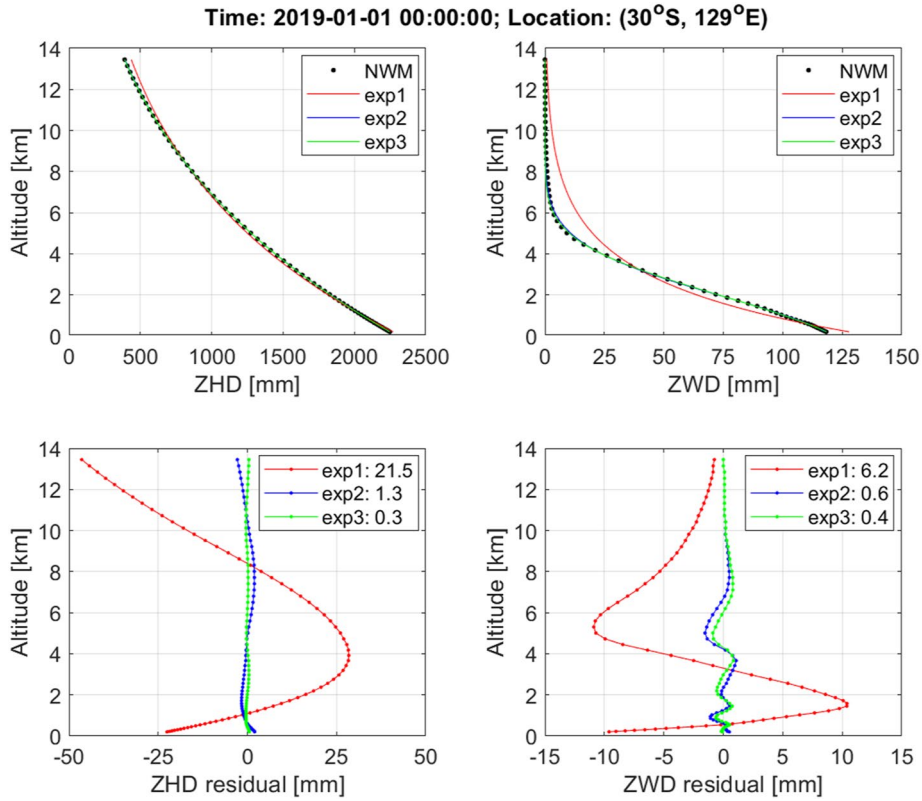

Figure 1. Tropospheric delay vertical profiles (black dots) and the exponential approximations (upper), and the fitting residuals (lower). Left: zenith hydrostatic delay (ZHD), right: zenith wet delay (ZWD). In the lower panels the root mean square (RMS) of residuals are shown in the legend. Note the different horizontal scales of different panels. The grid point location and time are given in the title.

When ignoring Equation 11 for fitting the delay profile, Equation 7 becomes a special case of Equation 10.

Therefore, we propose a simplified equation for the ZHD and ZWD vertical approximation:

$$ZD_h = ZD_0 \cdot e^{\Sigma_{i=1}^{n}(a_i \cdot h^i)}, \quad i = 1, 2, 3 \tag{12}$$

where ZD_0 and ZD_h indicate the zenith hydrostatic or wet delay at the surface and altitude h, respectively, and $(a_i, i = 1, 2, 3)$ are the coefficients to be fitted for ZHD and ZWD individually. When $i = 1$, this equation is equivalent with Equation 1; when $i = 2$ or $i = 3$, it is consistent with Equation 4 truncated at different orders. These three approximations are denoted as exp1, exp2, and exp3 in the following. We adopt Equation 12 instead of Equation 7 because it is more flexible to be linearized and fitted, free of the numerical issues, and can preserve better fitting precision.

Figure 1 gives an example of the vertical profiles of ZHD and ZWD obtained from the ERA5 model of European Centre for Medium-Range Weather Forecasts (ECMWF) (Hersbach et al., 2020) and the fitting results. We can clearly see large residuals of the exp1 solution, which are significantly smaller for exp2. For ZHD, the residuals of the exp1 solution can be up to 25 mm at the surface and at an altitude of about 4 km and the RMS is 21.5 mm. The residuals stay within ±3 mm from the surface up to 14 km altitude for the exp2 solution. As for ZWD, the absolute values of the residuals of the exp1 solution are about 10 mm at the surface, and about 2 and 5 km altitude, whereas the residuals of the exp2 solution stay within ±1 mm at all altitudes. The RMS of ZWD residuals reduces from 6.2 mm (exp1) to 0.6 mm (exp2). With RMS of 0.3 mm for ZHD and 0.4 mm for ZWD the tropospheric delay residuals of exp3 solution are even smaller.

2.3. The Empirical Tropospheric Delay Vertical Modeling

The current NWM-based tropospheric delays are provided in a two-dimensional global grid with the reference height corresponding to the Earth surface, and thus the model orography is always necessary. The height of most space geodetic reference points does not coincide with that of the model orography. The commonly used correction method (Kouba, 2007) takes the ZHD_h of a grid point with an altitude h, and calculates the corresponding pressure values employing Equation 6. Then the pressure value at the station height can be deduced as follows (Berg, 1948).

$$P_h = 1013.25 \cdot (1 - 0.0000226 \cdot h)^{5.225} \tag{13}$$

The ZHD at the station height is further derived from Equation 6.

As for ZWD, the following empirical model is used (Kouba, 2007).

$$ZWD_h = ZWD_{h_0} \cdot e^{-(h-h_0)/2000} \tag{14}$$

In this study we compare our method with this empirical model. Note that the empirical models are determined with historical data, whereas in our method the fitting coefficients are time-dependent, that is, one set of coefficients per epoch.

Despite these empirical correction methods, other analytical vertical scaling methods based on the meteorological data are also analyzed (see the supporting information), even though they are not used when implementing these NWM-derived tropospheric delay grids. The exponential functions outperform the analytical methods mainly due to the numerical fitting of all the coefficients. In such a set up further improvements may be introduced by including additional fitting coefficients.

3. Validating the Method

In this section the new method is analyzed using the NWM-based profiles in 2019. Using the ECMWF ERA5 hourly product with the horizontal resolution of $1° \times 1°$, we integrated ZHD and ZWD from the Earth surface (the lowest model level) to the altitude where ZWD vanishes. For the vertical resolution, we took the heights of the ERA5 profiles. We solely calculated the first epoch of each day, at 00:00 UT. The RMS of the residuals at each grid point was calculated and averaged over 2019. In addition, we calculated the RMS values of all the residuals at the lowest model level in 2019, that is, the modeling precision at the surface. In this study the Earth surface refers to the orography of ERA5.

3.1. Modeling Precision of Tropospheric Delay Profiles

Figure 2 shows the RMS values of the residuals of ZHD (left) and ZWD (right) obtained by solutions exp1, exp2, and exp3. For better visualization, we use different scales for the panels.

The RMS of ZHD fitting residuals (left panels of Figure 2) of exp1 solution is about 16.5–21.1 mm in most regions, and 21.1–23.5 mm in the North Atlantic Ocean, Mediterranean and Black Seas. With 5–12 mm, the smallest RMS values are observed in the high-altitude Antarctic Plateau (3 km average altitude) and Tibetan Plateau (4.5 km average altitude) and over Greenland. The RMS reduce to 1.8–2.7 mm in most regions with the exp2 solution, and to between 0.9 and 1.8 mm over land, for instance in West Asia, Africa, and Antarctic. However, larger RMS values up to 4 mm can still be observed in the Pacific Ocean west of South America. With the exp3 solution the RMS values further reduce to less than 2 mm in all the regions, and less than 1.1 mm at middle and lower latitudes. In summary, the exp1 solution cannot precisely model the ZHD vertical variation, highlighting the limitation of assuming a constant vertical temperature. By considering the temperature lapse rate, the modeling precision improves to 3 mm or less on a global scale for both solutions, exp2 and exp3.

For the ZWD fitting precision (right panels of Figure 2), the RMS shows obvious latitude dependence with larger values at the lower latitudes, as the lower latitude regions are characterized by higher water vapor content, and hence the vertical modeling is more difficult. The precision of the exp1 solution is better than 1.1 mm, 1.1–3.2 mm, and 3.2–5.3 mm at high, middle, and low latitudes, respectively; whereas that of the exp2 solution is less than 1.2 mm and 1.2–2.9 mm at higher and lower latitudes, respectively. With the exp3 solution the precision

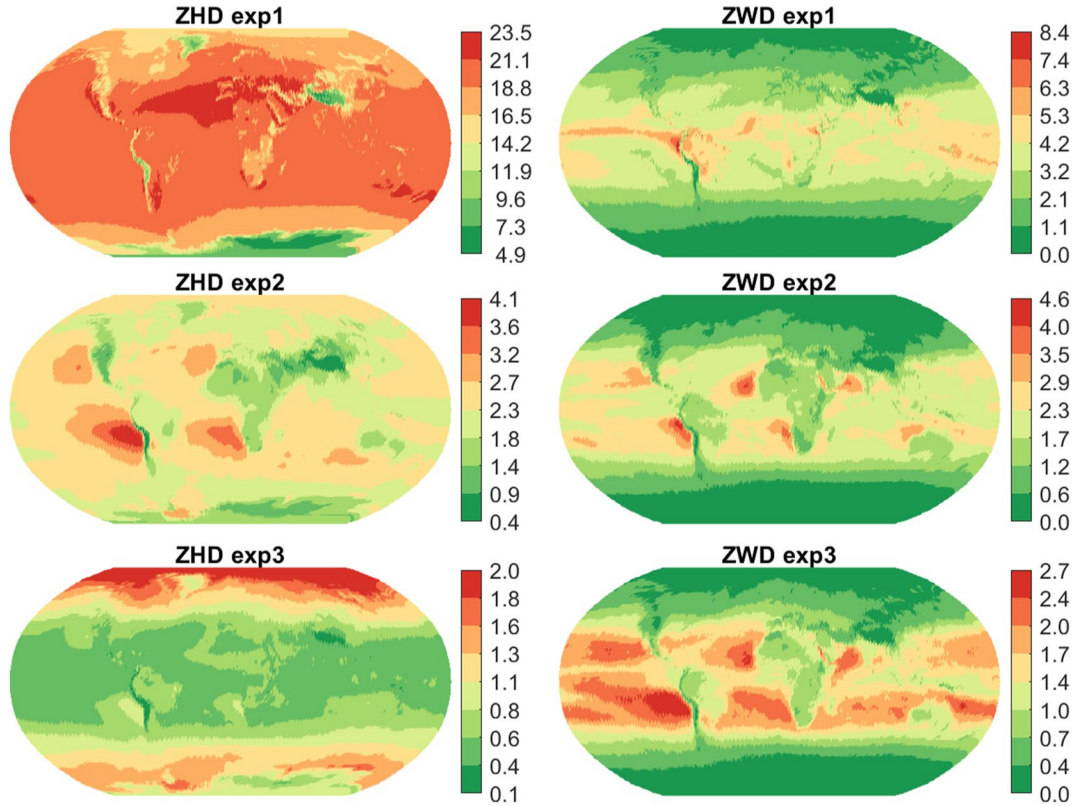

Figure 2. Average root mean square values of the vertical profile residuals of ZHD (left) and ZWD (right) using the exponential function with the order of one (top), two (middle), and three (bottom), during 2019. Units are mm. Note the different colorbar scales of the panels.

further improves reaching less than 2.7 mm globally and less than 1.0 mm at high latitudes. Note that for all three solutions, there are regions with relatively large RMS values, for instance, the west coast of South America.

3.2. Modeling Precision at the Earth Surface

As most space geodetic stations are located near the Earth surface, it is critical to ensure the modeling precision at the lowest level of the profiles. We thus present RMS values of the lowest NWM level during 2019 in Figure 3.

For the ZHD precision at surface shown in the left panels of Figure 3, the RMS is around 18.2–23.2 mm, 1.8–3.2 mm, and 0.5–1.2 mm for the epx1, exp2, and exp3 solutions, respectively. Nevertheless, for solution exp2 with about 5 mm the RMS can be relatively large in some regions, such as the west coast of South America, and 2–3 mm at the poles for solution exp3. As for ZWD (right panels of Figure 3), the precision is about 3.3–6.5 mm at lower latitudes and better than 3.3 mm at higher latitudes for solution exp1, better than 5.1 mm for solution exp2, and better than 3.2 mm for solution exp3. For both, hydrostatic and wet delays, the distribution of the precision at the surface is consistent with that of the whole vertical profiles, but the latter are better. Obviously, a precision of about 3 mm can be achieved at the Earth surface on a global scale using exp2 function, which is much better than that of exp1. The precision at the surface can be further improved down to 1–2 mm by the exp3 solution.

3.3. Modeling Precision at Different Latitudes and Altitudes

The modeling precision at different latitudes and altitudes is shown in Figure 4. For the altitude-dependent statistics, we calculated the RMS of the residuals at different altitude intervals, including that of the lowest NWM level (labeled "0"). For comparison, the precision of the empirical height correction method is also presented. We took the lowest level as reference, and calculated the hydrostatic and wet delays of each level up to 14 km height using the empirical approximation (see Section 2.3). The RMS values of the differences compared to the NWM-derived

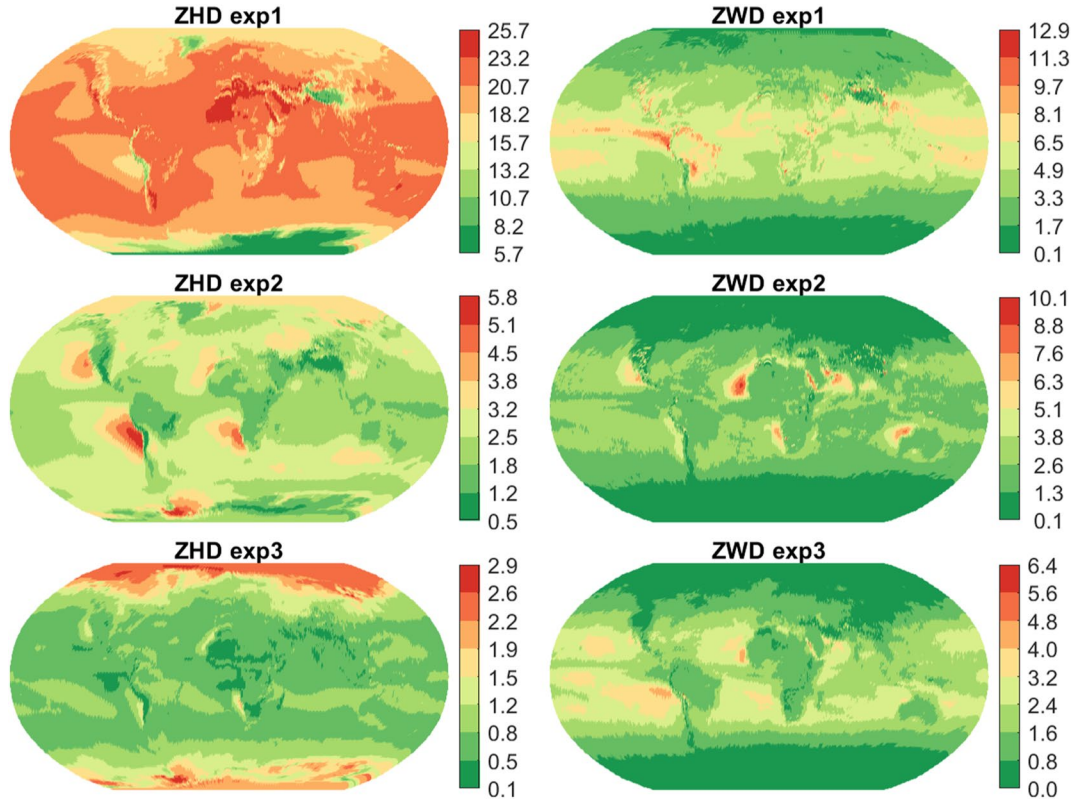

Figure 3. Average RMS values of the fitting residuals at the Earth surface (the lowest model level) for zenith hydrostatic delay (ZHD) (left) and zenith wet delay (ZWD) (right) using the exponential function with the order of one (upper), two (middle), and three (lower), in 2019. Units are mm. Note the different colorbar scales of the panels.

profiles are given in the emp columns in Figure 4. As for the latitude-dependent statistics, we calculated the average values of all the grid points from 90°S to 90°N with a step size of 20°, including the RMS values of both the vertical profiles and the surface, that is, the lowest model level.

The upper panels of Figure 4 show the altitude dependence of the modeling precision. For the hydrostatic delay, the average modeling precision of the vertical profiles (the [0, 14] columns) is 18.1, 2.2, and 1.0 mm for exp1, exp2, and exp3 solutions, respectively, and the corresponding RMS values at the surface (the "0" columns) are 18.9, 2.5, 1.2 mm. The precision of exp1 solutions varies significantly at different altitudes and the largest value of 25 mm is observed at the altitude of 8–14 km. As for the exp2 and exp3 solutions, the RMS values are always below 3 and 1.5 mm, respectively. The empirical model (emp) shows a good performance below 500 m with a precision of 3.6 mm, whereas the RMS value increases to 20–40 mm as the altitude increases to above 1 km. As for the wet delay, the average fitting precision of the profiles is 2.3, 1.3, and 0.9 mm for the epx1, exp2, and exp3 solutions, respectively, and that at the surface is 3.5, 1.7, and 1.4 mm, respectively. Unlike the hydrostatic delay, the wet delay fitting precision does not show large variation at different altitudes, except at 8–14 km where there is less water vapor and the wet delay tends to zero. The empirical model shows a precision of 2.8 mm below 500 m altitude, whereas the RMS value increases to 7–10 mm between 500 m and 5 km; above 5 km the RMS decreases significantly, due to the low water vapor content. The relatively better modeling precision of ZWD compared to ZHD is caused by the different magnitudes, that is, less than 0.4 m for ZWD compared to about 2.2 m for ZHD at the surface. In summary, the modeling precision of both, hydrostatic and wet delays, is significantly improved with the exp2 solution from the Earth surface to 14 km altitude, due to taking the temperature lapse rate into account. Further improvements can be observed for the exp3 solution, despite the small magnitude of around 1.2–1.3 mm and 0.3–0.4 mm for the hydrostatic and wet delays, respectively.

The lower panels of Figure 4 give the latitude dependence of the modeling precision. The modeling precision of hydrostatic delay of solution exp1 does not show a significant latitude dependence, in general. The RMS values

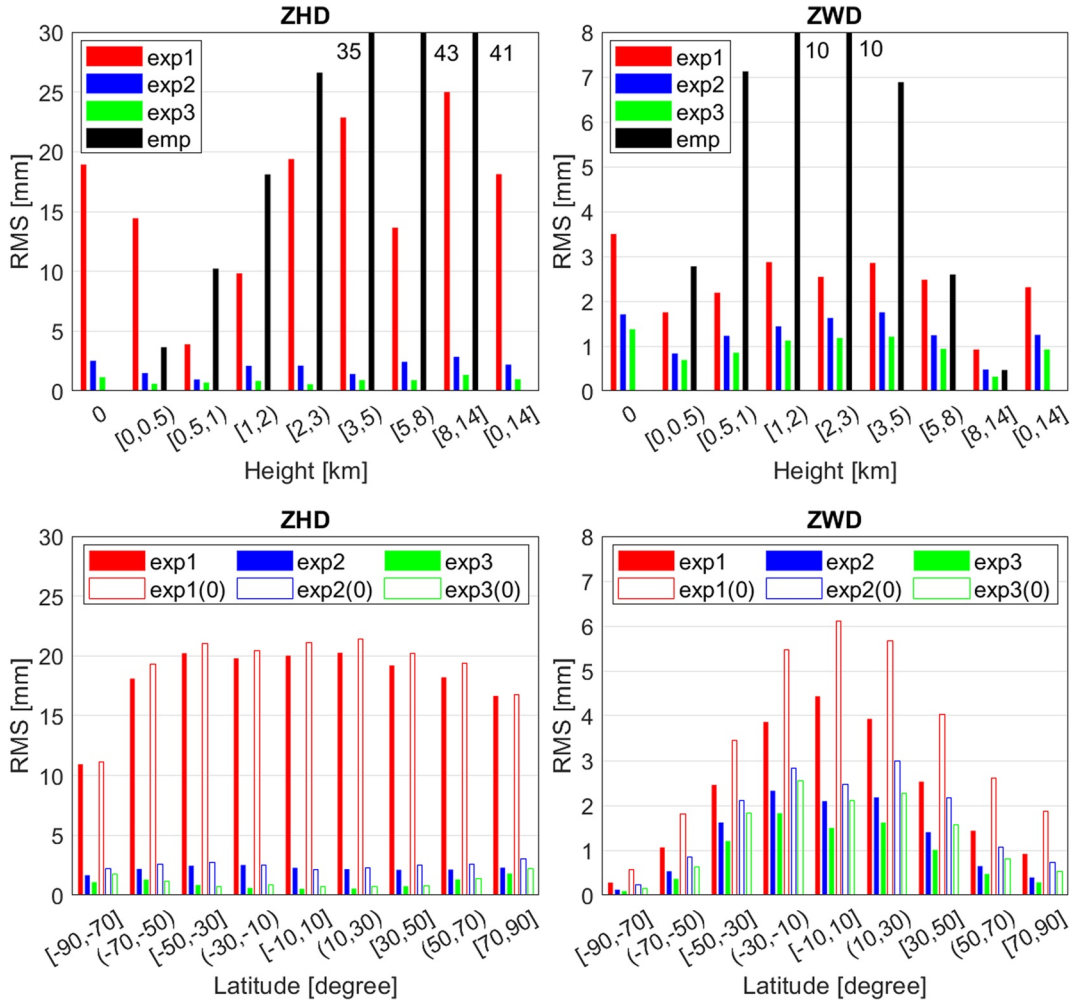

Figure 4. Modeling precision of zenith hydrostatic delay (ZHD) (left) and zenith wet delay (ZWD) (right) using the exponential functions with the order of one (exp1), two (exp2), and three (exp3) at different altitudes (upper) and different latitudes (lower). The average values during 2019 are presented. In the upper panels, the columns "0" show the precision at the Earth surface, and the black bars (emp) show the precision of the empirical model. More values are given in the text. In the lower panels, the statistics of exp1(0), exp2(0), and exp3(0) show the precision of the exponential function close to the Earth surface, with the order one, two, and three, respectively. Note the different vertical axes' scales for ZHD and ZWD.

are about 15–20 mm. An exception is the Antarctic region [90°S, 70°S], where the RMS is about 11 mm. The precision of exp2 solution has no significant differences at different latitudes, whereas that of the exp3 solution shows slightly better precision at lower latitudes (also see Figure S2 in Supporting Information S1). Across latitudes, the precision of hydrostatic delay at the surface is worse than that of the whole vertical profiles. For the wet delay, the modeling precision of all three solutions shows an obvious latitude dependence with much better precision at higher latitudes due to the relatively low water vapor content (see Figure S3 in Supporting Information S1 for the precision dependence on delay). The wet delay modeling precision close to the surface is also worse than that of the whole profile, which is consistent with the hydrostatic delay. Compared to the exp1 solution, the wet delay modeling precision improves through the exp2 and exp3 solutions gradually, especially at low latitudes. Taking the equatorial region [10°S, 10°N] as an example, the RMS is reduced from 4.4 mm (exp1) to 2.1 mm (exp2), and further to 1.5 mm (exp3), and the corresponding values at the surface are 6.1, 2.5, and 2.1 mm. To sum up both, hydrostatic and wet, delays at different latitudes can be precisely modeled when considering the temperature lapse rate (as it is the case for exp2 and exp3 solutions), and a precision of about 2 mm can be achieved even at lower latitudinal regions for the wet delay. The modeling precision, especially at lower altitudes, is further improved by the exp3 solution, which requires one more coefficient.

4. Conclusions and Perspectives

We presented a method to model the tropospheric delay vertical profiles from the Earth surface up to 14 km which preserves the NWM precision within 1–2 mm on the global scale. By considering the atmospheric temperature lapse rate and the time-dependency, the equation of the vertical function of atmospheric pressure is rearranged involving an exponent expanding into a power series of altitude. Both ZHD and ZWD from NWM can be precisely presented using three to four coefficients each. Compared to the linear exponent (constant vertical temperature), the second order exponential function improves the modeling precision by about 90% for hydrostatic delay and about 50% for wet delay. The second order exponential function shows consistent precision from the surface up to the height of 14 km. Thereby, our method is significantly better than the commonly used empirical correction method, especially at altitudes above 500 m. The modeling precision is consistent across latitudes for hydrostatic delays, but worse at low latitudes for the wet delays. Nevertheless, the NWM-determined ZWD can be represented within 2 mm even at the lower latitudes where the average amount of water vapor is typically high. The third order exponential function further improves the precision for both, the hydrostatic and wet delays, and ensures a precision better than 2 and 3 mm globally for the hydrostatic and wet delays, respectively. Note that our method aims at reducing the precision loss in delivering NWM-derived tropospheric delay, while the accuracy of original NWM data remains critical.

The proposed method can contribute significantly through providing an efficient NWM-derived tropospheric delay product to the space geodetic technique community ensuring a precision loss within 1–2 mm for both, hydrostatic and wet, delays from the Earth surface to the altitude of 14 km, covering also the altitude of airplanes (around 10 km). It is also computational cost inexpensive as the large number of NWM-based tropospheric delays are modeled with just three to four parameters. The method can be used to replace current ways of providing NWM-based tropospheric delays and qualifies for a wider range of users, especially for real-time kinematic GNSS applications in geohazard early warning systems.

Data Availability Statement

The ERA5 data set used in this study is publicly available at https://cds.climate.copernicus.eu/cdsapp#!/dataset/10.24381/cds.bd0915c6?tab=overview (Hersbach et al., 2020).

Acknowledgments
The authors thank ECMWF for providing the ERA5 data set, the Editor and anonymous reviewers for the valuable comments. Jungang Wang is funded by the Helmholtz OCPC Program (grant no. ZD202121). Kyriakos Balidakis is funded by the Deutsche Forschungsgemeinschaft (DFG) – Project-ID 434617780 – SFB 1464 (TerraQ). Xiao Chang is supported by the China Scholarship Council (grant no. 201703170248). Open access funding enabled and organized by Projekt DEAL.

References

Balidakis, K., Nilsson, T., Zus, F., Glaser, S., Heinkelmann, R., Deng, Z., & Schuh, H. (2018). Estimating integrated water vapor trends from VLBI, GPS, and numerical weather models: Sensitivity to tropospheric parameterization. *Journal of Geophysical Research: Atmospheres*, *123*(12), 6356–6372. https://doi.org/10.1029/2017jd028049

Berberan-Santos, M. N., Bodunov, E. N., & Pogliani, L. (1997). On the barometric formula. *American Journal of Physics*, *65*(5), 404–412. https://doi.org/10.1119/1.18555

Berg, H. (1948). *Allgemeine meteorologie*. Duemmler.

Blewitt, G., Hammond, W., & Kreemer, C. (2018). Harnessing the GPS data explosion for interdisciplinary science. *Eos*, *99*. https://doi.org/10.1029/2018eo104623

Böhm, J., & Schuh, H. (2013). *Atmospheric effects in space geodesy* (Vol. XVII, p. 234). Springer-Verlag Berlin Heidelberg.

Böhm, J., Werl, B., & Schuh, H. (2006). Troposphere mapping functions for GPS and very long baseline interferometry from European Centre for Medium-Range Weather Forecasts operational analysis data. *Journal of Geophysical Research: Solid Earth*, *111*(B2). https://doi.org/10.1029/2005jb003629

Davis, J. L., Herring, T. A., Shapiro, I. I., Rogers, A. E. E., & Elgered, G. (1985). Geodesy by radio interferometry: Effects of atmospheric modeling errors on estimates of baseline length. *Radio Science*, *20*(6), 1593–1607. https://doi.org/10.1029/RS020i006p01593

de Oliveira, P. S., Morel, L., Fund, F., Legros, R., Monico, J. F. G., Durand, S., & Durand, F. (2016). Modeling tropospheric wet delays with dense and sparse network configurations for PPP-RTK. *GPS Solutions*, *21*(1), 237–250. https://doi.org/10.1007/s10291-016-0518-0

Dousa, J., & Elias, M. (2014). An improved model for calculating tropospheric wet delay. *Geophysical Research Letters*, *41*(12), 4389–4397. https://doi.org/10.1002/2014gl060271

Emardson, T. R., & Jarlemark, P. O. J. (1999). Atmospheric modelling in GPS analysis and its effect on the estimated geodetic parameters. *Journal of Geodesy*, *73*(6), 322–331. https://doi.org/10.1007/s001900050249

Eriksson, D., MacMillan, D. S., & Gipson, J. M. (2014). Tropospheric delay ray tracing applied in VLBI analysis. *Journal of Geophysical Research: Solid Earth*, *119*(12), 9156–9170. https://doi.org/10.1002/2014jb011552

Fernandes, M. J., Lázaro, C., Ablain, M., & Pires, N. (2015). Improved wet path delays for all ESA and reference altimetric missions. *Remote Sensing of Environment*, *169*, 50–74. https://doi.org/10.1016/j.rse.2015.07.023

Fernandes, M. J., Lázaro, C., & Vieira, T. (2021). On the role of the troposphere in satellite altimetry. *Remote Sensing of Environment*, *252*, 112149. https://doi.org/10.1016/j.rse.2020.112149

Foster, J., Brooks, B., Cherubini, T., Shacat, C., Businger, S., & Werner, C. L. (2006). Mitigating atmospheric noise for InSAR using a high resolution weather model. *Geophysical Research Letters*, *33*(16). https://doi.org/10.1029/2006gl026781

Foster, J. H., Carter, G. S., & Merrifield, M. A. (2009). Ship-based measurements of sea surface topography. *Geophysical Research Letters*, *36*(11). https://doi.org/10.1029/2009gl038324

Grapenthin, R., Johanson, I., & Allen, R. M. (2014). The 2014 Mw 6.0 Napa earthquake, California: Observations from real-time GPS-enhanced earthquake early warning. *Geophysical Research Letters*, *41*, 8269–8276. https://doi.org/10.1002/2014GL061923

Hadas, T., Kaplon, J., Bosy, J., Sierny, J., & Wilgan, K. (2013). Near-real-time regional troposphere models for the GNSS precise point positioning technique. *Measurement Science and Technology*, *24*(5), 055003. https://doi.org/10.1088/0957-0233/24/5/055003

Heinkelmann, R., Böhm, J., Bolotin, S., Engelhardt, G., Haas, R., Lanotte, R., et al. (2011). VLBI-derived troposphere parameters during CONT08. *Journal of Geodesy*, *85*(7), 377–393. https://doi.org/10.1007/s00190-011-0459-x

Hersbach, H., Bell, B., Berrisford, P., Hirahara, S., Horányi, A., Muñoz-Sabater, J., et al. (2020). The ERA5 global reanalysis. *Quarterly Journal of the Royal Meteorological Society*, *146*(730), 1999–2049. https://doi.org/10.1002/qj.3803

Hobiger, T., Ichikawa, R., Koyama, Y., & Kondo, T. (2008). Fast and accurate ray-tracing algorithms for real-time space geodetic applications using numerical weather models. *Journal of Geophysical Research*, *113*(D20). https://doi.org/10.1029/2008jd010503

Hofmeister, A., & Böhm, J. (2017). Application of ray-traced tropospheric slant delays to geodetic VLBI analysis. *Journal of Geodesy*, *91*(8), 945–964. https://doi.org/10.1007/s00190-017-1000-7

Hreinsdóttir, S., Sigmundsson, F., Roberts, M., Björnsson, H., Grapenthin, R., Arason, P., et al. (2014). Volcanic plume height correlated with magma-pressure change at Grímsvötn Volcano, Iceland. *Nature Geoscience*, *7*, 214–218. https://doi.org/10.1038/ngeo2044

Kouba, J. (2007). Implementation and testing of the gridded Vienna mapping function 1 (VMF1). *Journal of Geodesy*, *82*(4–5), 193–205. https://doi.org/10.1007/s00190-007-0170-0

Landskron, D., & Böhm, J. (2019). Improving dUT1 from VLBI intensive sessions with GRAD gradients and ray-traced delays. *Advances in Space Research*, *63*(11), 3429–3435. https://doi.org/10.1016/j.asr.2019.03.041

Lee, S.-W., Yun, S.-H., Kim, D. H., Lee, D., Lee, Y. J., & Schutz, B. E. (2015). Real-time volcano monitoring using GNSS single-frequency receivers. *Journal of Geophysical Research: Solid Earth*, *120*, 8551–8569. https://doi.org/10.1002/2014JB011648

Legeais, J. F., Ablain, M., & Thao, S. (2014). Evaluation of wet troposphere path delays from atmospheric reanalyses and radiometers and their impact on the altimeter sea level. *Ocean Science*, *10*(6), 893–905. https://doi.org/10.5194/os-10-893-2014

Lente, G., & Ősz, K. (2020). Barometric formulas: Various derivations and comparisons to environmentally relevant observations. *ChemTexts*, *6*(2). https://doi.org/10.1007/s40828-020-0111-6

Lu, C., Li, X., Zus, F., Heinkelmann, R., Dick, G., Ge, M., et al. (2017). Improving BeiDou real-time precise point positioning with numerical weather models. *Journal of Geodesy*, *91*(9), 1019–1029. https://doi.org/10.1007/s00190-017-1005-2

Nilsson, T., Soja, B., Balidakis, K., Karbon, M., Heinkelmann, R., Deng, Z., & Schuh, H. (2017). Improving the modeling of the atmospheric delay in the data analysis of the Intensive VLBI sessions and the impact on the UT1 estimates. *Journal of Geodesy*, *91*(7), 857–866. https://doi.org/10.1007/s00190-016-0985-7

Penna, N. T., Morales Maqueda, M. A., Martin, I., Guo, J., & Foden, P. R. (2018). Sea surface height measurement using a GNSS wave glider. *Geophysical Research Letters*, *45*(11), 5609–5616. https://doi.org/10.1029/2018gl077950

Rocken, C., Johnson, J., Van Hove, T., & Iwabuchi, T. (2005). Atmospheric water vapor and geoid measurements in the open ocean with GPS. *Geophysical Research Letters*, *32*(12). https://doi.org/10.1029/2005GL022573

Ruhl, C. J., Melgar, D., Grapenthin, R., & Allen, R. M. (2017). The value of real-time GNSS to earthquake early warning. *Geophysical Research Letters*, *44*, 8311–8319. https://doi.org/10.1002/2017GL074502

Saastamoinen, J. (1972). Atmospheric correction for the troposphere and stratosphere in radio ranging satellites. In S. W. Henriksen, A. Mancini, & B. H. Chovitz (Eds.), *The use of artificial satellites for geodesy* (pp. 247–251). https://doi.org/10.1029/GM015P0247

Sobolev, S., Babeyko, A., Wang, R., Galas, R., Rothacher, M., Lauterjung, J., et al. (2006). Towards real-time tsunami amplitude prediction. *Eos Trans. AGU*, *87*(37), 374–378. https://doi.org/10.1029/2006EO370003

Soja, B., Nilsson, T., Karbon, M., Zus, F., Dick, G., Deng, Z., et al. (2015). Tropospheric delay determination by Kalman filtering VLBI data. *Earth Planets and Space*, *67*(1). https://doi.org/10.1186/s40623-015-0293-0

Takeichi, N., Sakai, T., Fukushima, S., & Ito, K. (2009). Tropospheric delay correction with dense GPS network in L1-SAIF augmentation. *GPS Solutions*, *14*(2), 185–192. https://doi.org/10.1007/s10291-009-0133-4

Tsushima, H., Hino, R., Ohta, Y., Iinuma, T., & Miura, S. (2014). tFISH/RAPiD: Rapid improvement of near-field tsunami forecasting based on offshore tsunami data by incorporating onshore GNSS data. *Geophysical Research Letters*, *41*, 3390–3397. https://doi.org/10.1002/2014GL059863

Urquhart, L., Nievinski, F. G., & Santos, M. C. (2013). Assessment of troposphere mapping functions using three-dimensional ray-tracing. *GPS Solutions*, *18*(3), 345–354. https://doi.org/10.1007/s10291-013-0334-8

Vaclavovic, P., Dousa, J., Elias, M., & Kostelecky, J. (2017). Using external tropospheric corrections to improve GNSS positioning of hot-air balloon. *GPS Solutions*, *21*(4), 1479–1489. https://doi.org/10.1007/s10291-017-0628-3

Wang, J., & Liu, Z. (2019). Improving GNSS PPP accuracy through WVR PWV augmentation. *Journal of Geodesy*, *93*(9), 1685–1705. https://doi.org/10.1007/s00190-019-01278-2

Wang, J., Wu, Z., Semmling, M., Zus, F., Gerland, S., Ramatschi, M., et al. (2019). Retrieving precipitable water vapor from shipborne multi-GNSS observations. *Geophysical Research Letters*, *46*(9), 5000–5008. https://doi.org/10.1029/2019gl082136

Ware, R. H., Rocken, C., & Hurst, K. J. (1986). A Global Positioning System baseline determination including bias fixing and water vapor radiometer corrections. *Journal of Geophysical Research*, *91*(B9), 9183. https://doi.org/10.1029/JB091iB09p09183

Webb, S. R., Penna, N. T., Clarke, P. J., Webster, S., Martin, I., & Bennitt, G. V. (2016). Kinematic GNSS estimation of zenith wet delay over a range of altitudes. *Journal of Atmospheric and Oceanic Technology*, *33*(1), 3–15. https://doi.org/10.1175/jtech-d-14-00111.1

Wilgan, K., & Geiger, A. (2018). High-resolution models of tropospheric delays and refractivity based on GNSS and numerical weather prediction data for alpine regions in Switzerland. *Journal of Geodesy*, *93*(6), 819–835. https://doi.org/10.1007/s00190-018-1203-6

Wilgan, K., Hadas, T., Hordyniec, P., & Bosy, J. (2017). Real-time precise point positioning augmented with high-resolution numerical weather prediction model. *GPS Solutions*, *21*(3), 1341–1353. https://doi.org/10.1007/s10291-017-0617-6

Yu, C., Li, Z., Penna, N. T., & Crippa, P. (2018). Generic atmospheric correction model for interferometric synthetic aperture radar observations. *Journal of Geophysical Research: Solid Earth*, *123*(10), 9202–9222. https://doi.org/10.1029/2017jb015305

Zheng, F., Lou, Y., Gu, S., Gong, X., & Shi, C. (2017). Modeling tropospheric wet delays with national GNSS reference network in China for BeiDou precise point positioning. *Journal of Geodesy*, *92*(5), 545–560. https://doi.org/10.1007/s00190-017-1080-4

Zhou, Y., Lou, Y., Zhang, W., Kuang, C., Liu, W., & Bai, J. (2020). Improved performance of ERA5 in global tropospheric delay retrieval. *Journal of Geodesy*, *94*(10). https://doi.org/10.1007/s00190-020-01422-3

Zus, F., Dick, G., Douša, J., Heise, S., & Wickert, J. (2014). The rapid and precise computation of GPS slant total delays and mapping factors utilizing a numerical weather model. *Radio Science*, *49*(3), 207–216. https://doi.org/10.1002/2013rs005280